UCSF
UC San Francisco Previously Published Works

Title
The oncogene cyclin D1 promotes bipolar spindle integrity under compressive force

Permalink
https://escholarship.org/uc/item/0bh1s0vs

Journal
PLOS ONE, 19(3)

ISSN
1932-6203

Authors
Sutanto, Renaldo
Neahring, Lila
Marques, Andrea Serra
et al.

Publication Date
2024

DOI
10.1371/journal.pone.0296779

Copyright Information
This work is made available under the terms of a Creative Commons Attribution License, available at https://creativecommons.org/licenses/by/4.0/

Peer reviewed

eScholarship.org Powered by the California Digital Library
University of California

PLOS ONE

RESEARCH ARTICLE

The oncogene cyclin D1 promotes bipolar spindle integrity under compressive force

Renaldo Sutanto[1☯¤a], **Lila Neahring**[1,2☯¤b]*, **Andrea Serra Marques**[1¤c], **Mauricio Jacobo Jacobo**[1,3,4], **Seda Kilinc**[3¤d], **Andrei Goga**[3,5,6], **Sophie Dumont**[1,2,7,8]*

1 Department of Bioengineering & Therapeutic Sciences, University of California San Francisco, San Francisco, California, United States of America, **2** Developmental & Stem Cell Biology Graduate Program, University of California San Francisco, San Francisco, California, United States of America, **3** Department of Cell & Tissue Biology, University of California San Francisco, San Francisco, California, United States of America, **4** Pharmaceutical Sciences and Pharmacogenomics Graduate Program, University of California San Francisco, San Francisco, California, United States of America, **5** Helen Diller Family Comprehensive Cancer Center, University of California San Francisco, San Francisco, California, United States of America, **6** Department of Medicine, University of California San Francisco, San Francisco, California, United States of America, **7** Department of Biochemistry & Biophysics, University of California San Francisco, San Francisco, California, United States of America, **8** Chan Zuckerberg Biohub, San Francisco, California, United States of America

☯ These authors contributed equally to this work.
¤a Current address: Cell & Developmental Biology Graduate Program, University of Michigan, Ann Arbor, Michigan, United States of America
¤b Current address: Developmental Biology Program, Sloan Kettering Institute, New York, New York, United States of America
¤c Current address: Genentech, South San Francisco, California, United States of America
¤d Current address: Exai Bio, Palo Alto, California, United States of America
* lila.neahring@ucsf.edu (LN); sophie.dumont@ucsf.edu (SD)

Abstract

The mitotic spindle is the bipolar, microtubule-based structure that segregates chromosomes at each cell division. Aberrant spindles are frequently observed in cancer cells, but how oncogenic transformation affects spindle mechanics and function, particularly in the mechanical context of solid tumors, remains poorly understood. Here, we constitutively overexpress the oncogene cyclin D1 in human MCF10A cells to probe its effects on spindle architecture and response to compressive force. We find that cyclin D1 overexpression increases the incidence of spindles with extra poles, centrioles, and chromosomes. However, it also protects spindle poles from fracturing under compressive force, a deleterious outcome linked to multipolar cell divisions. Our findings suggest that cyclin D1 overexpression may adapt cells to increased compressive stress, possibly contributing to its prevalence in cancers such as breast cancer by allowing continued proliferation in mechanically challenging environments.

OPEN ACCESS

Citation: Sutanto R, Neahring L, Serra Marques A, Jacobo Jacobo M, Kilinc S, Goga A, et al. (2024) The oncogene cyclin D1 promotes bipolar spindle integrity under compressive force. PLoS ONE 19(3): e0296779. https://doi.org/10.1371/journal.pone.0296779

Editor: Daniela Cimini, Virginia Tech, UNITED STATES

Received: August 2, 2023

Accepted: December 19, 2023

Published: March 13, 2024

Copyright: © 2024 Sutanto et al. This is an open access article distributed under the terms of the Creative Commons Attribution License, which permits unrestricted use, distribution, and reproduction in any medium, provided the original author and source are credited.

Data Availability Statement: All relevant data used to generate plots are included in the Supporting Information files.

Funding: This work was supported by a National Science Foundation Graduate Research Fellowship, Fannie and John Hertz Foundation Fellowship, and the UCSF Discovery Fellows Program (L.N.); NIH R35GM136420, NSF 1548297 Center for Cellular Construction, the Chan Zuckerberg Initiative, and the UCSF Byers Award (S.D.); NIH R01CA266756, CDMRP W81XWH-21-1-0774, the Mark

Introduction

The spindle is the macromolecular machine that segregates chromosomes at each cell division. In mammalian cells, mitotic spindles are bipolar structures with one centrosome at each

Foundation for Cancer Research and Atwater Family Foundation (A.G.); and NIH 5T32CA108462 (S.K.). The funders had no role in study design, data collection and analysis, decision to publish, or preparation of the manuscript.

Competing interests: The authors have declared that no competing interests exist.

spindle pole. Errors in cell division are associated with genomic instability and disease, and aberrant spindles are hallmarks of cancer [1]. Extra centrosomes [2–4], continuously evolving karyotypes known as chromosomal instability [5, 6], and multipolar spindles are elevated in tumors across many tissues of origin and diverse cancer genotypes. Oncogenes can also induce defects in spindle assembly even in the absence of gross spindle abnormalities; for example, MYC overexpression prolongs mitosis and increases chromosome segregation errors [7]. Paradoxically, while such multipolar, clustered pseudo-bipolar, or otherwise aberrant spindles are generally adverse for mitotic outcomes [8, 9], they can promote tumorigenesis by increasing genetic diversity [1] and potentially other unknown mechanisms. How oncogenic transformation affects spindle assembly remains poorly understood.

Dividing cells in solid tumors are subject to dramatically different mechanical environments than their counterparts in healthy tissue [10–12]. Spindle poles in dividing cultured cells often fracture under compressive force, leading to mitotic delays, multipolar anaphases, and subsequent cell death [13–16]. Tumors have been shown to be confining microenvironments due to their increased cell density, elevated interstitial fluid pressure [17], and increased extracellular matrix deposition and crosslinking [18], raising the question of how cells continue to divide under this high compressive stress. In breast tumors, compressive stress is high enough to deform and damage interphase nuclei [19], and nearby mitotic cells presumably experience similarly high forces that may interfere with mitotic rounding or spindle assembly. In multicellular tumor spheroid models, compressive stress reduces cell proliferation [20–23] and has been shown to disrupt bipolar spindle assembly in cells that continue to divide [24]. Due to the challenges of making controlled mechanical perturbations at the cellular scale, the mechanisms underlying the spindle's mechanical integrity remain poorly understood [25]. Little is known about whether and how the spindles of transformed cells mechanically differ from wild-type spindles as they adapt to the tumor environment.

Cyclin D1, overexpressed in 50–70% of breast cancers [26], is an oncogene with pleiotropic effects in the cell. Acute overexpression of cyclin D1 leads to spindle and karyotypic defects [27], and long-term overexpression is sufficient to drive breast cancer in mice [28]. In addition to its canonical role in complex with CDK4/6 in controlling cell cycle progression at the G1/S transition, cyclin D1 may contribute to tumorigenesis through its roles in cytoskeletal remodeling and CDK-independent transcriptional programs [26]. Many other oncogenes commonly dysregulated in breast cancer, such as Ras and ErbB2, are upstream of cyclin D1 [29–31], making cyclin D1 overexpression a good model to probe changes in spindle mechanics after oncogenic transformation.

Here, we compare control and cyclin D1-overexpressing breast epithelial cells to investigate their spindle architectures and responses to compressive stress. We find that cyclin D1 increases the proportion of spindles containing extra poles, chromosomes, and centrosomes. However, cyclin D1 overexpression also promotes bipolar spindle integrity during cell compression, preventing spindle pole fracture that results in multipolar cell divisions. We propose that cyclin D1 overexpression mechanically adapts cell division to compressive environments, potentially contributing to its prevalence in cancer despite the aberrant spindles it induces.

Results

Constitutive cyclin D1 overexpression promotes aberrant spindle architectures

To determine the effects of cyclin D1 overexpression on spindle architecture, we compared MCF10A breast epithelial cell lines stably overexpressing cyclin D1 or a puromycin resistance gene as a control [32]. The parental MCF10A cells are diploid and non-transformed, but are

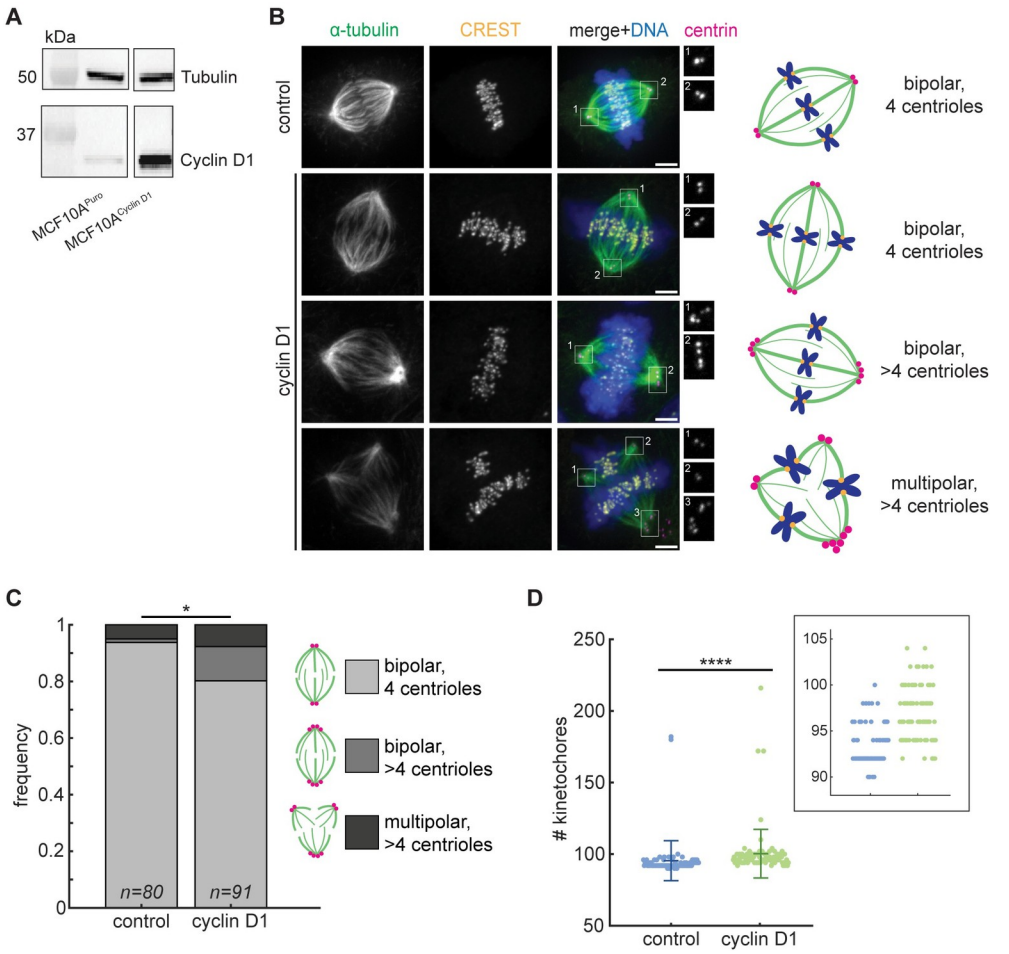

Fig 1. Cyclin D1 overexpression promotes aberrant spindle architectures. (A) Western blot of α-tubulin and cyclin D1 levels in $MCF10A^{Puro}$ (control) and $MCF10A^{Cyclin\ D1}$ cell lines. All images are from the same blot, with intervening lanes removed. (B) Representative confocal immunofluorescence images (maximum intensity projections) of spindles stained for α-tubulin (green), CREST (yellow), centrin (magenta), and Hoechst (blue), with spindle phenotypes cartooned (right). Magnifications of the centrioles at each spindle pole are shown at right. Scale bars = 3 μm. (C) Frequency of the three observed metaphase spindle phenotypes in each MCF10A cell line. The distribution of phenotypes differs between cyclin D1 and control cells (*p = 0.010, Fisher's exact test), with the cyclin D1 line enriched in cells with supernumerary centrioles. (D) Number of kinetochores per spindle. Metaphase spindles in the cyclin D1 cell line had significantly more kinetochores (representing the number of chromatids) than the control line (****$p = 2.32 \times 10^{-14}$, Mann-Whitney U test). Lines indicate mean ± standard deviation. Inset shows a smaller range of kinetochore numbers. For C and D, n = 80 control spindles and 91 cyclin D1 spindles, each pooled from 3 independent experiments.

https://doi.org/10.1371/journal.pone.0296779.g001

sensitive to transformation by a variety of oncogenes [32–34]. We confirmed overexpression of cyclin D1 by western blot (Fig 1A), and used immunofluorescence to quantify spindle pole, centriole, and kinetochore numbers by staining for α-tubulin, centrin, and CREST respectively (Fig 1B).

While most control spindles (94%) had two centrioles at each of two spindle poles, supernumerary centrioles were more common in the cyclin D1-expressing cells (20% of cells; Fig 1C). These centrioles were either associated with multipolar spindles or clustered into pseudo-bipolar spindles, a known mechanism by which cancer cells adapt to extra centrosomes in order to avoid multipolar divisions [35–37].

To gain insight into cyclin D1's effect on genomic integrity, we next counted the kinetochores in each spindle. Several mechanisms, including the clustering of extra centrosomes [8, 9] and reduced kinetochore-microtubule dynamics [38], have been shown to give rise to aneuploidy and chromosomal instability in cancer cells, while cytokinesis failure leads to larger-scale genomic duplications. Cyclin D1 overexpression was associated with a broader range of chromosome numbers than in controls, with only a small number of cells containing a near-doubling of chromosome number, indicating that it induces aneuploidy (Fig 1D). The average chromosome number increased from 95.4 in control cells to 100.3 in cyclin D1-overexpressing cells, a level of aneuploidy that we do not expect to affect spindle size. In summary, constitutive overexpression of the oncogene cyclin D1 leads to an increased incidence of spindles with extra poles, centrioles, and chromosomes, even when cells are allowed to adapt to elevated cyclin D1 over many passages.

Cyclin D1 overexpression promotes bipolar spindle integrity under compressive stress

Although we observed that cyclin D1 overexpression gave rise to higher rates of spindle defects in cultured cells (Fig 1), cyclin D1 is known to be overexpressed in many tumors such as breast cancers. Because cells in breast tumors have also been reported to be subject to increased compressive stress [12, 19, 26], we wondered whether cyclin D1 may be adaptive in the context of a compressive solid tumor. Thus, we hypothesized that cyclin D1 overexpression might alter the spindle's biophysical properties to improve mitotic outcomes in cells dividing under compressive stress. We compared the mechanical robustness of control versus cyclin D1-overexpressing spindles by compressing cells in PDMS-based microfluidic devices and performing live imaging (Fig 2A) [39]. Cells were pre-treated with the proteasome inhibitor MG132 to prevent anaphase entry, allowing us to focus on the metaphase spindle's response to compressive stress, and gradually compressed to a final height of 5 μm via a computer-controlled vacuum pump over 4 minutes. Compression was then sustained for an additional 70 minutes. This perturbation was reproducible from cell to cell, reducing spindle height from an average of 10.55 ± 1.54 μm to 4.72 ± 0.31 μm (mean ± standard deviation of all cells) (Fig 2B and 2C). Spindles in control and cyclin D1-overexpressing cells had indistinguishable average heights prior to compression and were compressed to a similar final height (Fig 2C). Spindles also widened and elongated as compression was applied, consistent with previous work [40–42]. Spindle lengths before compression were similar between the control and cyclin D1 cells, as were spindle lengths at 10 minutes post-compression onset, when spindle shape had stabilized (Fig 2D). Spindles were wider in control cells vs. cyclin D1-overexpressing cells, both before and after compression, but the difference was slight (Fig 2E). Thus, our assay probes how cyclin D1 overexpression affects the spindle's intrinsic ability to adapt to a well-defined confined geometry, rather than probing cellular shape change in response to a defined compressive stress.

During compression experiments, we monitored changes in spindle integrity in addition to changes in spindle shape. Control spindle poles fractured into multiple foci during the 74 minutes of compression 47.4% of the time, with kinetochore-fibers detaching and splaying laterally from the original spindle pole (Fig 3A and 3B; S1 Movie). Interestingly, bipolar spindles in the cyclin D1-overexpressing line fractured significantly less often, in just 20.8% of compressions (Fig 3B; S2 Movie). Although these spindles experienced similar compression-induced deformations, most spindles maintained all kinetochore-fibers focused into the two original spindle poles.

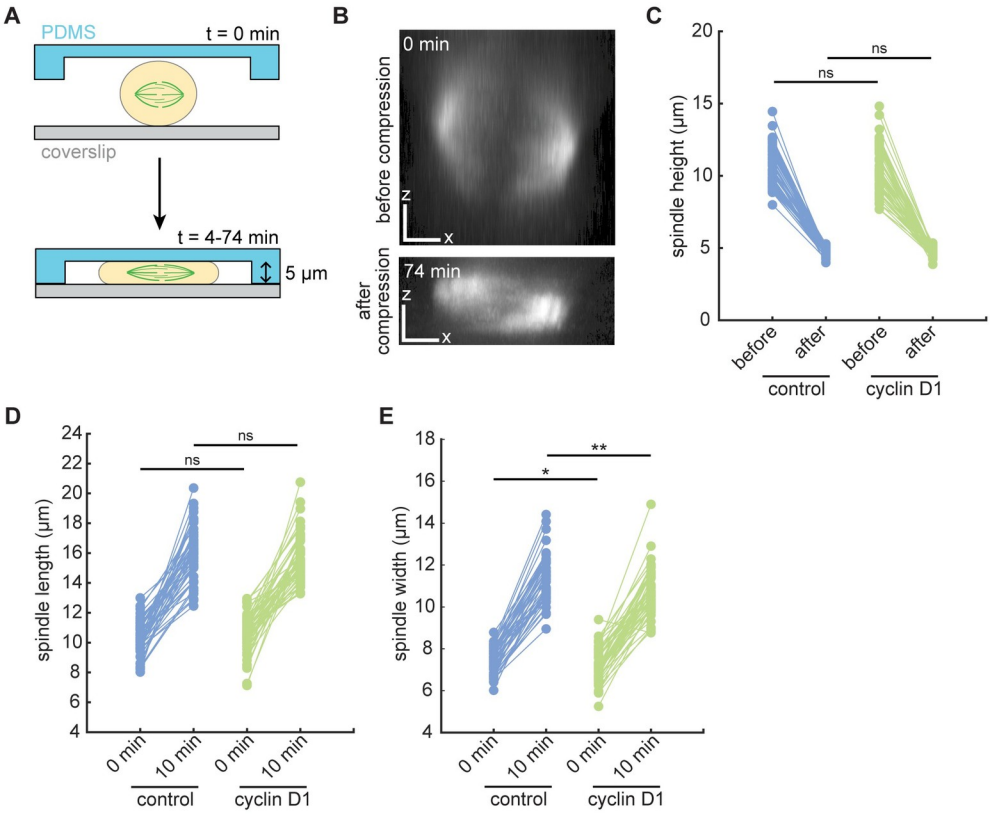

Fig 2. The cell compression assay is quantitatively reproducible. (A) Schematic diagram of cell compression assay using a microfluidic device. Cells were compressed to a height of 5 μm using computer-controlled negative pressure over 4 min, and compression was sustained for 70 additional minutes. Cells were live-imaged throughout to monitor changes in spindle architecture. (B) Side (XZ) views of a control spindle, labeled with SiR-tubulin, before and after (at 74 min) compression. X and Z scale bars = 3 μm. (C) Between the control and cyclin D1 cell lines, spindle heights did not significantly differ before compression, and spindles were compressed to a similar final height (measured at 74 min). ns, not significant. (D) Spindle lengths before and 10 minutes after compression onset (ns, not significant). (E) Spindle widths before and 10 minutes after compression onset (*p = 0.028, **p = 0.00066). For C-E, two-sample t-tests were performed with n = 57 control and 53 cyclin D1 spindles (C) or n = 48 control and 52 cyclin D1 spindles (D and E), pooled from 13 and 12 independent days, respectively. Spindles were excluded from length and width analysis if both poles were not in focus in the same z-plane.

https://doi.org/10.1371/journal.pone.0296779.g002

To probe the consequences of spindle pole fracture, we imaged control cell compressions without the addition of MG132 to follow spindles into late mitosis. Fractured spindles were still able to progress to anaphase, but they segregated chromosomes into three or more masses, depending on the number of new poles created by fracture (Fig 3C; S3 Movie; note the example shown was compressed using 4 μm micropillars). Interestingly, poles that separated from each other as a result of fracture were directly connected by few or no microtubules (Fig 3C, white arrow), and cytokinetic furrowing between these fractured poles was delayed and possibly incomplete (Fig 3C, yellow arrow).

Finally, we compared the levels of several spindle pole proteins—NuMA, HSET, Aurora A kinase, and TACC3—in the two cell lines, to test whether any were differentially regulated as a consequence of cyclin D1 overexpression. Each of these proteins localizes to spindle poles, and they play roles in assembling and maintaining the spindle pole (NuMA) [43–45], clustering supernumerary centrosomes (HSET) [37], phosphorylating other spindle proteins and localizing them to the pole (Aurora A kinase) [46], and regulating microtubule dynamics at

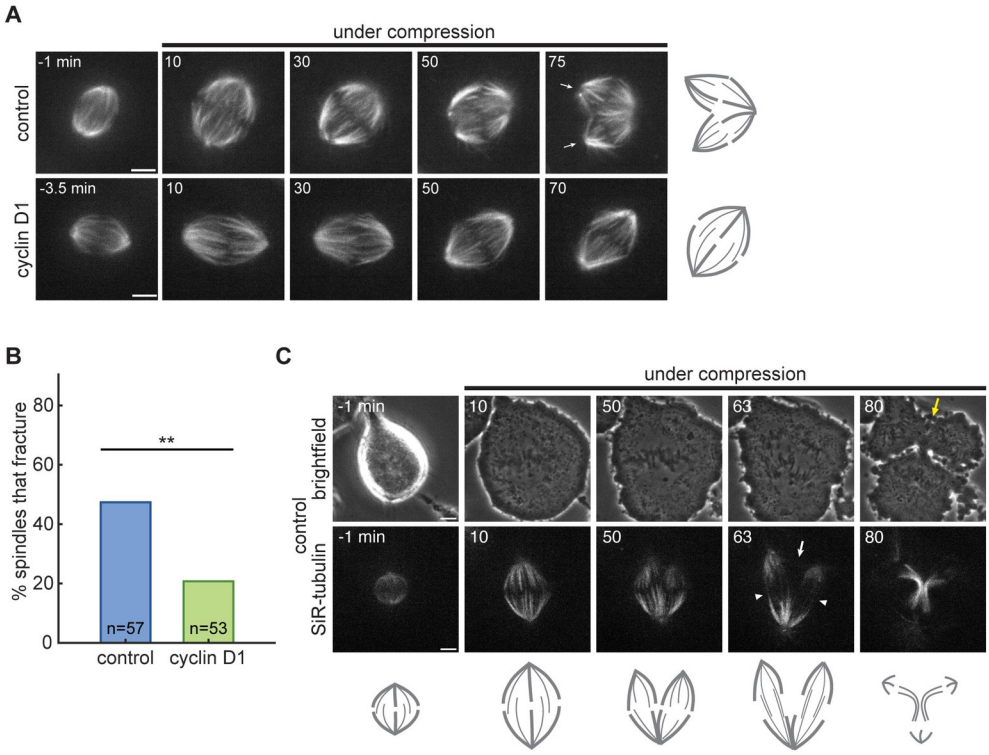

Fig 3. Cyclin D1 overexpression protects against spindle pole fracture during compression. (A) Confocal time-lapse images of control and cyclin D1-overexpressing cells undergoing compression, where the control spindle fractures around 60 min after compression onset (cartooned at right). The fractured poles of the control spindle are indicated in the final frame by white arrows. Tubulin is labeled with SiR-tubulin. Scale bars = 5 μm; time stamps are in minutes. (B) Spindles in cyclin D1-overexpressing cells fractured less often than control spindles during the 74 minutes of compression (**p = 0.0048, Fisher's exact test). n = 57 control and 53 cyclin D1 spindles pooled from 13 and 12 independent days, respectively. (C) Confocal time-lapse images of a control spindle undergoing compression to a height of 4 μm, without the addition of MG132. After the spindle fractures between the 10 and 50 min time points, the cell enters anaphase and segregates chromosomes into 3 masses (cartooned below). Interpolar microtubule bundles connect the original pole to each of the fractured poles (white arrowheads), while no interpolar bundles connect the two poles resulting from the fracture (white arrow). The cytokinetic furrow is disrupted between the two fractured poles by the final 80 min timepoint (yellow arrow). Scale bars = 5 μm; time stamps are in minutes.

https://doi.org/10.1371/journal.pone.0296779.g003

centrosomes (TACC3) [47, 48]. We found that NuMA, but none of the other candidates tested, was upregulated in the cyclin D1 cell line (Fig 4A–4C), suggesting that NuMA could mediate cyclin D1's effect on pole robustness. Our results suggest that compressive force on mitotic MCF10A cells often causes spindle poles to fracture, leading to abnormal chromosome segregation at anaphase, but that overexpression of the oncogene cyclin D1 is protective against spindle fracture.

Discussion

Many oncogenes induce aberrant spindle architectures, yet they also promote uncontrolled cell proliferation in tumorigenesis. One explanation for this apparent paradox is that the elevated rate of chromosome mis-segregation in these spindles accelerates genome evolution and gives some cells a selective advantage [49]. Here, we describe another mechanism by which an oncogene could act as a double-edged sword, with detrimental consequences for the cell in some contexts but conferring a proliferative advantage in others. Overexpression of cyclin D1 increases the prevalence of mitotic cells containing extra poles, centrioles, and chromosomes

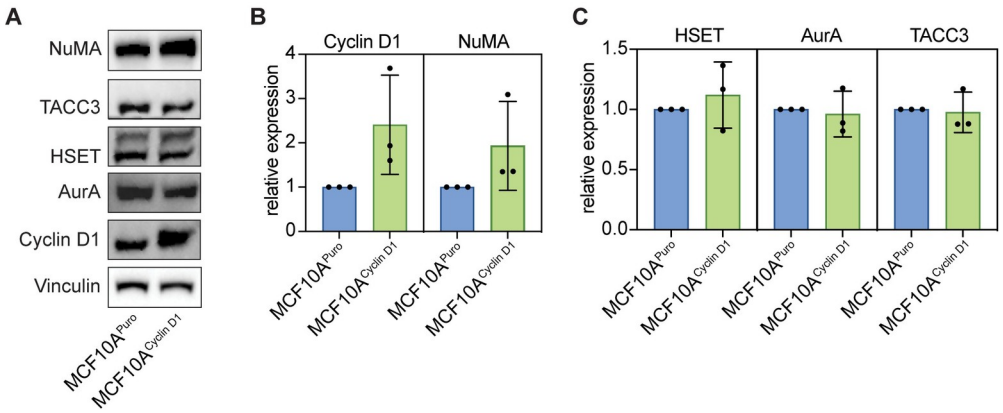

Fig 4. NuMA, but not HSET, Aurora A kinase, or TACC3, is upregulated in cyclin D1-overexpressing cells. (A) Western blot of NuMA, TACC3, HSET, Aurora A kinase, and cyclin D1 levels in MCF10A^{Puro} (control) and MCF10A$^{Cyclin\ D1}$ cell lines. The overexpressed cyclin D1 is HA-tagged. Vinculin is shown as a loading control. (B-C) Quantification of NuMA, cyclin D1 (B), HSET, Aurora A kinase, and TACC3 levels (C) normalized to vinculin levels. Lines show mean ± standard deviation of three independent replicates.

https://doi.org/10.1371/journal.pone.0296779.g004

(Fig 1), but also reduces the frequency of spindle fracture under compressive stress (Figs 2 and 3). Our assay was conducted in two-dimensional culture and with compressive force that may differ in magnitude and direction from that experienced by cells in vivo. Indeed, a recent study using HeLa cells found that while confinement-induced cell flattening led to increased pole fracturing, confining cells into elongated, narrow channels was protective against pole fracturing [16]. However, an increase in spindle multipolarity has also been observed in confined HCT116 colorectal cancer cell spheroids [24], suggesting that our assay mimics compressive forces that exist in a crowded three-dimensional environment.

Although the fractured spindles we followed into anaphase segregated chromosomes into more than two masses (Fig 3C), many of these mitoses presumably resolved into two daughter cells due to the lack of an anaphase central spindle competent to recruit the cytokinetic machinery between the newly separated poles. However, rapid nuclear envelope reformation at mitotic exit may prevent these multiple DNA masses from merging and lead to genomic instability or cell cycle arrest. Because cyclin D1 overexpression has a protective effect on bipolar spindle integrity under compressive force, we propose that it helps to prevent multipolar anaphases and speculate that it may allow cells to continue proliferating under compressive stress in the tumor context. Intriguingly, the cyclin D1 interactors pRb, p27, and p21 have been shown to mediate a G1 arrest in cells subjected to compressive stress [22, 23, 50], suggesting that cyclin D1 levels may affect the likelihood both that cells will continue to divide under compression and that they will complete these divisions successfully.

This work poses the question of the mechanisms by which cyclin D1 overexpression protects against spindle fracture. We find that cyclin D1-overexpressing cells upregulate NuMA (Fig 4). A role for NuMA in mediating the pole-protective effect downstream of cyclin D1 would be consistent with NuMA's function of clustering microtubule minus ends at spindle poles [44, 45], and with previous observations that it promotes pole integrity under compressive stress [42]. Cyclin D1 could directly or indirectly regulate additional factors involved in the cell's or the spindle's response to compression through its kinase-dependent or transcriptional roles [26]. These factors could be regulated by cyclin D1 during interphase, and we note that cyclin D1 itself need not be expressed at high levels during mitosis. Pharmacologically inhibiting CDK4/6, the partner kinases of cyclin D1, and testing whether spindles in cyclin D1-overexpressing cells are sensitized to compressive stress could help determine whether

cyclin D1's pole protective effect is kinase dependent. Any effects of CDK4/6 inhibitors on spindle mechanics may also be therapeutically relevant, because these inhibitors are widely used to treat metastatic estrogen receptor-positive breast cancer [51].

Indirect consequences of cyclin D1 overexpression could also underlie the spindle pole protection we observe. Incomplete mitotic rounding has been shown to lead to pole fracturing [14], and oncogenic h-Ras^{G12V} has been shown to prevent pole fracture in MCF10A cells by enhancing mitotic rounding under stiff gels [15]. We propose that different mechanisms are at play in the protective effect we observe here, because spindles in cyclin D1-overexpressing cells underwent fewer fractures despite being compressed to the same flattened height as spindles in control cells (Fig 2C). Supernumerary centrioles could contribute to the protective effect of cyclin D1 by increasing the density of microtubules and/or pericentriolar material at poles [2, 52, 53]. Indeed, the proportion of bipolar spindles containing extra centrioles was increased from 1.3% of controls to 13.1% in the cyclin D1 cell line (Fig 1C), and whether the pole-protective effect of cyclin D1 occurs specifically in cells with centriole amplification is an important question. Finally, other proteins that are differentially regulated during oncogenic transformation (but not specifically downstream of cyclin D1) could affect pole integrity. Future work dissecting the mechanism(s) by which cyclin D1 promotes bipolar spindle integrity under compression will be important to predict how generalizable this phenomenon is likely to be among tumors with diverse driver oncogenes. More broadly, achieving this goal will require a better understanding of the physical and molecular basis of spindle mechanical integrity [54–56].

The biochemical hallmarks of cancer, including anti-apoptotic signaling, metabolic reprogramming, and cell cycle dysregulation, are well-established [57]. By contrast, our knowledge of the biophysical hallmarks of cancer lags behind, and addressing this gap could reveal new insights into disease progression. Our application of controlled, cellular-scale force suggests that cyclin D1 overexpression may adapt dividing cells to the mechanical burdens of the tumor environment. Better understanding the biophysical adaptations of cancer cells could lead to new ways to selectively target these cells for therapeutic gain.

Materials and methods

Cell culture

MCF10A^{PURO} and MCF10A$^{CYCLIN\ D1}$ cells were created in a previous study [32]. Both cell lines were cultured at 37˚C and 5% CO_2, and maintained in DMEM/F12 (Invitrogen) supplemented with 5% horse serum (Gibco), 20 ng/ml epidermal growth factor (Sigma), 10 μg/ml insulin (Sigma), 0.5 μg/ml hydrocortisone (Sigma), 100 ng/ml cholera toxin (Millipore), and 100 U/ml penicillin and streptomycin (Gibco). For immunofluorescence experiments, cells were plated on 25 mm round #1.5 coverslips, coated with poly-L-lysine (Sigma) and 0.1% gelatin solution (from Type B 2% solution, Sigma), two days prior to fixation. For compression experiments, cells were plated in 35 mm petri dishes containing 23 mm #1.5 poly-D-lysine-coated coverslips (World Precision Instruments) two days prior to imaging. Cells were plated to achieve a confluency of ~40–50% at imaging, to allow space for cells to expand under compression.

Western blotting

Cells in 6-well plates were lysed, and protein extracts were collected after centrifugation at 4˚C for 30 min. Protein concentrations were measured using a Bradford assay, and equal concentrations of each sample were separated on a 4–12% Bis-Tris gel (Invitrogen) by SDS-PAGE and transferred to a nitrocellulose membrane. Membranes were blocked with 4% milk, incubated in primary antibodies overnight at 4˚C, and incubated with HRP-conjugated secondary

antibodies for 1 hour. Proteins were detected using SuperSignal West Pico or Femto chemiluminescent substrates (Thermo Fisher). The following primary antibodies were used: mouse anti-α-tubulin DM1α (1:5,000, Sigma-Aldrich T6199), rabbit anti-cyclin D1 SP4 (1:1,000, Abcam ab16663), rabbit anti-cyclin D1 E3P5S (1:1,000, Cell Signaling 55506), rabbit anti-TACC3 D9E4 (1:1,000, Cell Signaling 8069), rabbit anti-Aurora A kinase (1:1,000, Cell Signaling 3092), rabbit anti-NuMA (1:1,000, Novus NB500-174), mouse anti-KIFC1 M-63 (1:1,000, Santa Cruz Biotechnology sc-100947), and rabbit anti-Vinculin E1E9V (1:10,000, Cell Signaling 13901). The following secondary antibodies were used at a 1:10,000 dilution: goat anti-mouse IgG-HRP (Santa Cruz Biotechnology sc-2005) and mouse anti-rabbit IgG-HRP (Santa Cruz Biotechnology sc-2357).

Immunofluorescence

Cells were fixed in cold methanol for 2 minutes at -20˚C. Cells were washed in TBST (0.05% Triton-X 100 in TBS) and blocked with 2% BSA in TBST. Primary and secondary antibodies were diluted in TBST + 2% BSA and incubated for one hour at room temperature (primary antibodies) or 50 minutes at room temperature (secondary antibodies). DNA was labeled with 1 μg/ml Hoechst 33342 prior to mounting on slides with ProLong Gold Antifade Mountant (Thermo Fisher P36934). The following primary antibodies were used: mouse anti-α-tubulin DM1α conjugated to Alexa Fluor 488 (1:100, Cell Signaling Technologies 8058S), mouse anti-centrin clone 20H5 (1:200, Sigma-Aldrich 04–1624), and human anti-centromere protein CREST antibody (1:25, Antibodies Incorporated 15–234). Normal mouse IgG (1:100, Santa Cruz Biotechnology sc-2025) was used as a block before incubating in pre-conjugated mouse anti-α-tubulin DM1α Alexa Fluor 488. The following secondary antibodies were used: goat anti-mouse conjugated to Alexa Fluor 488 and 568 (1:400, Invitrogen A11001 and A11004) and goat anti-human conjugated to Alexa Fluor 647 (1:400, Invitrogen A21445).

Cell compression

Cell compressions were performed using a 1-well dynamic cell confiner with 5 μm PDMS micropillars, or 4 μm micropillars for the example shown in Fig 3C (4DCell). The device was attached to an AF1 Dual vacuum/pressure controller (Elveflow) and negative pressure was controlled using the Elveflow ESI software. Prior to imaging, a seal was established between the compression device and the dish of cells by applying a negative pressure of -10 mbar. At the start of imaging, a linear pressure ramp was applied from -10 to -150 mbar over a period of 4 minutes to lower the pillared coverslip onto the cells. Once the PDMS pillars contacted the dish, compression was maintained for 70 minutes. Z-stacks were acquired before each compression and after each timelapse acquisition to determine spindle height before and after each compression and quantitatively compare compression outcomes.

Imaging

Live imaging experiments were conducted in a stage-top humidified incubation chamber (Tokai Hit WSKM) maintained at 37˚C and 5% CO_2. In compression experiments, microtubules were labeled with 100 nM SiR-tubulin (Cytoskeleton, Inc.) and 10 μM verapamil for 30–60 minutes prior to imaging. For all compression experiments shown except for the example in Fig 3C, the proteasome inhibitor MG132 was added to a final concentration of 10 μM 10 minutes prior to imaging to prevent anaphase entry during compressions. All live and immunofluorescence imaging was performed on an inverted spinning disk confocal (CSU-X1, Yokogawa Electric Corporation) microscope (Eclipse Ti-E, Nikon) with the following components: head dichroic Semrock Di01-T405/488/568/647; 405 nm (100 mW), 488 nm (150 mW),

561 nm (100 mW), and 642 nm (100 mW) diode lasers; ET455/50M, ET525/50M, ET600/50M, ET690/50M, and ET705/72M emission filters (Chroma Technology); and a Zyla 4.2 sCMOS camera (Andor Technology). Exposures of 50–200 ms were used for fluorescence. Images were acquired with a 100× 1.45 NA Ph3 oil objective using MetaMorph 7.7.8.0 (Molecular Devices).

Data and statistical analysis

Immunofluorescence images show maximum intensity projections (Fig 1B) and time strip images show single spinning disk confocal Z-slices (Fig 3). All images were formatted for publication using FIJI [58]. The brightness/contrast for each channel was scaled identically between different example cells for immunofluorescence images. The brightness/contrast for videos and time strips were scaled individually to account for variations in tubulin labeling efficiency. Kinetochores were counted using the multi-point tool in FIJI. For compression experiments, spindle heights were measured from XZ views generated from z-stacks (see Fig 2B) in a vertical direction perpendicular to the coverslip. A fracture was defined as the development of a clear gap in tubulin intensity between a kinetochore-fiber minus-end and the main spindle pole within 74 minutes of compression onset (Fig 3).

Fisher's exact test was used to compare categorical datasets (Figs 1C and 3B); two-sample t-tests were used to compare the numerical datasets in Fig 2C–2E based on the assumption that spindle heights, lengths, and widths are approximately normally distributed; and a Mann-Whitney U test was used to compare the numerical dataset in Fig 1D due to kinetochore number distributions that deviated from a normal distribution. Statistical tests were performed using the ttest2, ranksum, and fishertest functions in MATLAB R2022b, and the fisher.test function in R for the 2x3 comparison in Fig 1C. All statistical tests were two-sided. P-values are given in the figure legends.

Supporting information

S1 Movie. A control cell before and after compression. Time stamps are in min:sec, scale bars are 5 μm, and video playback is 30 frames per second. See also Fig 3A.
(MP4)

S2 Movie. A cyclin D1-overexpressing cell before and after compression. Time stamps are in min:sec, scale bars are 5 μm, and video playback is 30 frames per second. See also Fig 3A.
(MP4)

S3 Movie. A control cell before and after compression to a height of 4 μm, without the addition of MG132. Time stamps are in min:sec, scale bars are 5 μm, and video playback is 30 frames per second. See also Fig 3C.
(MP4)

S1 Raw images. Raw images of all western blots.
(PDF)

S1 File. Source data for all graphs.
(XLSX)

Acknowledgments

We thank Rachel Nakagawa and Julia Rohrberg for experimental advice, and other members of the Goga and Dumont labs for helpful discussions.

Author Contributions

Conceptualization: Lila Neahring, Andrei Goga, Sophie Dumont.

Data curation: Renaldo Sutanto, Lila Neahring, Andrea Serra Marques, Mauricio Jacobo Jacobo.

Formal analysis: Renaldo Sutanto, Lila Neahring, Mauricio Jacobo Jacobo.

Funding acquisition: Andrei Goga, Sophie Dumont.

Investigation: Renaldo Sutanto, Lila Neahring, Andrea Serra Marques, Mauricio Jacobo Jacobo.

Methodology: Renaldo Sutanto, Lila Neahring, Andrea Serra Marques, Andrei Goga, Sophie Dumont.

Resources: Lila Neahring, Seda Kilinc, Andrei Goga.

Supervision: Lila Neahring, Andrei Goga, Sophie Dumont.

Validation: Renaldo Sutanto, Lila Neahring, Andrea Serra Marques, Sophie Dumont.

Visualization: Renaldo Sutanto, Lila Neahring, Mauricio Jacobo Jacobo.

Writing – original draft: Lila Neahring.

Writing – review & editing: Renaldo Sutanto, Lila Neahring, Andrea Serra Marques, Seda Kilinc, Andrei Goga, Sophie Dumont.

References

1. Holland AJ, Cleveland DW. Boveri revisited: chromosomal instability, aneuploidy and tumorigenesis. Nat Rev Mol Cell Biol. 2009; 10(7):478–87. https://doi.org/10.1038/nrm2718 PMID: 19546858
2. Lingle WL, Lutz WH, Ingle JN, Maihle NJ, Salisbury JL. Centrosome hypertrophy in human breast tumors: implications for genomic stability and cell polarity. Proc Natl Acad Sci U S A. 1998; 95(6):2950–5. https://doi.org/10.1073/pnas.95.6.2950 PMID: 9501196
3. Pihan GA, Purohit A, Wallace J, Knecht H, Woda B, Quesenberry P, et al. Centrosome defects and genetic instability in malignant tumors. Cancer Res. 1998; 58(17):3974–85. PMID: 9731511
4. Chan JY. A clinical overview of centrosome amplification in human cancers. Int J Biol Sci. 2011; 7 (8):1122–44. Epub https://doi.org/10.7150/ijbs.7.1122 PMID: 22043171.
5. Lengauer C, Kinzler KW, Vogelstein B. Genetic instability in colorectal cancers. Nature. 1997; 386 (6625):623–7. https://doi.org/10.1038/386623a0 PMID: 9121588
6. Drews RM, Hernando B, Tarabichi M, Haase K, Lesluyes T, Smith PS, et al. A pan-cancer compendium of chromosomal instability. Nature. 2022; 606(7916):976–83. Epub 20220615. https://doi.org/10.1038/s41586-022-04789-9 PMID: 35705807
7. Rohrberg J, Van de Mark D, Amouzgar M, Lee JV, Taileb M, Corella A, et al. MYC Dysregulates Mitosis, Revealing Cancer Vulnerabilities. Cell Rep. 2020; 30(10):3368–82 e7. https://doi.org/10.1016/j.celrep.2020.02.041 PMID: 32160543
8. Ganem NJ, Godinho SA, Pellman D. A mechanism linking extra centrosomes to chromosomal instability. Nature. 2009; 460(7252):278–82. Epub https://doi.org/10.1038/nature08136 PMID: 19506557.
9. Silkworth WT, Nardi IK, Scholl LM, Cimini D. Multipolar spindle pole coalescence is a major source of kinetochore mis-attachment and chromosome mis-segregation in cancer cells. PLoS One. 2009; 4(8): e6564. Epub 20090810. https://doi.org/10.1371/journal.pone.0006564 PMID: 19668340
10. Kumar S, Weaver VM. Mechanics, malignancy, and metastasis: the force journey of a tumor cell. Cancer Metastasis Rev. 2009; 28(1–2):113–27. https://doi.org/10.1007/s10555-008-9173-4 PMID: 19153673
11. Plodinec M, Loparic M, Monnier CA, Obermann EC, Zanetti-Dallenbach R, Oertle P, et al. The nanomechanical signature of breast cancer. Nat Nanotechnol. 2012; 7(11):757–65. Epub https://doi.org/10.1038/nnano.2012.167 PMID: 23085644.

12. Nia HT, Liu H, Seano G, Datta M, Jones D, Rahbari N, et al. Solid stress and elastic energy as measures of tumour mechanopathology. Nat Biomed Eng. 2016;1. Epub 20161128. https://doi.org/10.1038/s41551-016-0004 PMID: 28966873

13. Tse HT, Weaver WM, Di Carlo D. Increased asymmetric and multi-daughter cell division in mechanically confined microenvironments. PLoS One. 2012; 7(6):e38986. Epub 20120625. https://doi.org/10.1371/journal.pone.0038986 PMID: 22761717

14. Lancaster OM, Le Berre M, Dimitracopoulos A, Bonazzi D, Zlotek-Zlotkiewicz E, Picone R, et al. Mitotic rounding alters cell geometry to ensure efficient bipolar spindle formation. Dev Cell. 2013; 25(3):270–83. Epub 20130425. https://doi.org/10.1016/j.devcel.2013.03.014 PMID: 23623611

15. Matthews HK, Ganguli S, Plak K, Taubenberger AV, Win Z, Williamson M, et al. Oncogenic Signaling Alters Cell Shape and Mechanics to Facilitate Cell Division under Confinement. Dev Cell. 2020; 52(5):563–73 e3. Epub 20200206. https://doi.org/10.1016/j.devcel.2020.01.004 PMID: 32032547

16. Cheng L, Li J, Sun H, Jiang H. Appropriate mechanical confinement inhibits multipolar cell division via pole-cortex interaction. Physical Review X. 2023; 13(1). https://doi.org/10.1103/PhysRevX.13.011036

17. Heldin CH, Rubin K, Pietras K, Ostman A. High interstitial fluid pressure—an obstacle in cancer therapy. Nat Rev Cancer. 2004; 4(10):806–13. https://doi.org/10.1038/nrc1456 PMID: 15510161

18. Levental KR, Yu H, Kass L, Lakins JN, Egeblad M, Erler JT, et al. Matrix crosslinking forces tumor progression by enhancing integrin signaling. Cell. 2009; 139(5):891–906. https://doi.org/10.1016/j.cell.2009.10.027 PMID: 19931152

19. Nader GPF, Aguera-Gonzalez S, Routet F, Gratia M, Maurin M, Cancila V, et al. Compromised nuclear envelope integrity drives TREX1-dependent DNA damage and tumor cell invasion. Cell. 2021; 184(20):5230–46 e22. Epub 20210921. https://doi.org/10.1016/j.cell.2021.08.035 PMID: 34551315

20. Helmlinger G, Netti PA, Lichtenbeld HC, Melder RJ, Jain RK. Solid stress inhibits the growth of multicellular tumor spheroids. Nat Biotechnol. 1997; 15(8):778–83. https://doi.org/10.1038/nbt0897-778 PMID: 9255794

21. Cheng G, Tse J, Jain RK, Munn LL. Micro-environmental mechanical stress controls tumor spheroid size and morphology by suppressing proliferation and inducing apoptosis in cancer cells. PLoS One. 2009; 4(2):e4632. Epub 20090227. https://doi.org/10.1371/journal.pone.0004632 PMID: 19247489

22. Delarue M, Montel F, Vignjevic D, Prost J, Joanny JF, Cappello G. Compressive stress inhibits proliferation in tumor spheroids through a volume limitation. Biophys J. 2014; 107(8):1821–8. https://doi.org/10.1016/j.bpj.2014.08.031 PMID: 25418163

23. Taubenberger AV, Girardo S, Traber N, Fischer-Friedrich E, Krater M, Wagner K, et al. 3D Microenvironment Stiffness Regulates Tumor Spheroid Growth and Mechanics via p21 and ROCK. Adv Biosyst. 2019; 3(9):e1900128. Epub 20190724. https://doi.org/10.1002/adbi.201900128 PMID: 32648654

24. Desmaison A, Frongia C, Grenier K, Ducommun B, Lobjois V. Mechanical stress impairs mitosis progression in multi-cellular tumor spheroids. PLoS One. 2013; 8(12):e80447. Epub 20131203. https://doi.org/10.1371/journal.pone.0080447 PMID: 24312473

25. Valdez VA, Neahring L, Petry S, Dumont S. Mechanisms underlying spindle assembly and robustness. Nat Rev Mol Cell Biol. 2023. Epub 20230328. https://doi.org/10.1038/s41580-023-00584-0 PMID: 36977834

26. Musgrove EA, Caldon CE, Barraclough J, Stone A, Sutherland RL. Cyclin D as a therapeutic target in cancer. Nat Rev Cancer. 2011; 11(8):558–72. Epub 20110707. https://doi.org/10.1038/nrc3090 PMID: 21734724

27. Nelsen CJ, Kuriyama R, Hirsch B, Negron VC, Lingle WL, Goggin MM, et al. Short term cyclin D1 overexpression induces centrosome amplification, mitotic spindle abnormalities, and aneuploidy. J Biol Chem. 2005; 280(1):768–76. Epub 20041026. https://doi.org/10.1074/jbc.M407105200 PMID: 15509582

28. Wang TC, Cardiff RD, Zukerberg L, Lees E, Arnold A, Schmidt EV. Mammary hyperplasia and carcinoma in MMTV-cyclin D1 transgenic mice. Nature. 1994; 369(6482):669–71. https://doi.org/10.1038/369669a0 PMID: 8208295

29. Lee RJ, Albanese C, Fu M, D'Amico M, Lin B, Watanabe G, et al. Cyclin D1 is required for transformation by activated Neu and is induced through an E2F-dependent signaling pathway. Mol Cell Biol. 2000; 20(2):672–83. https://doi.org/10.1128/MCB.20.2.672-683.2000 PMID: 10611246

30. Yu Q, Geng Y, Sicinski P. Specific protection against breast cancers by cyclin D1 ablation. Nature. 2001; 411(6841):1017–21. https://doi.org/10.1038/35082500 PMID: 11429595

31. Desai KV, Xiao N, Wang W, Gangi L, Greene J, Powell JI, et al. Initiating oncogenic event determines gene-expression patterns of human breast cancer models. Proc Natl Acad Sci U S A. 2002; 99(10):6967–72. https://doi.org/10.1073/pnas.102172399 PMID: 12011455

32. Martins MM, Zhou AY, Corella A, Horiuchi D, Yau C, Rakhshandehroo T, et al. Linking tumor mutations to drug responses via a quantitative chemical-genetic interaction map. Cancer Discov. 2015; 5(2):154–67. Epub 20141212. https://doi.org/10.1158/2159-8290.CD-14-0552 PMID: 25501949

33. Soule HD, Maloney TM, Wolman SR, Peterson WD Jr., Brenz R, McGrath CM, et al. Isolation and characterization of a spontaneously immortalized human breast epithelial cell line, MCF-10. Cancer Res. 1990; 50(18):6075–86. PMID: 1975513

34. Debnath J, Mills KR, Collins NL, Reginato MJ, Muthuswamy SK, Brugge JS. The role of apoptosis in creating and maintaining luminal space within normal and oncogene-expressing mammary acini. Cell. 2002; 111(1):29–40. https://doi.org/10.1016/s0092-8674(02)01001-2 PMID: 12372298

35. Ring D, Hubble R, Kirschner M. Mitosis in a cell with multiple centrioles. J Cell Biol. 1982; 94(3):549–56. https://doi.org/10.1083/jcb.94.3.549 PMID: 7130271

36. Quintyne NJ, Reing JE, Hoffelder DR, Gollin SM, Saunders WS. Spindle multipolarity is prevented by centrosomal clustering. Science. 2005; 307(5706):127–9. https://doi.org/10.1126/science.1104905 PMID: 15637283

37. Kwon M, Godinho SA, Chandhok NS, Ganem NJ, Azioune A, Thery M, et al. Mechanisms to suppress multipolar divisions in cancer cells with extra centrosomes. Genes Dev. 2008; 22(16):2189–203. Epub 20080728. https://doi.org/10.1101/gad.1700908 PMID: 18662975

38. Bakhoum SF, Thompson SL, Manning AL, Compton DA. Genome stability is ensured by temporal control of kinetochore-microtubule dynamics. Nat Cell Biol. 2009; 11(1):27–35. Epub 20081207. https://doi.org/10.1038/ncb1809 PMID: 19060894

39. Le Berre M, Zlotek-Zlotkiewicz E, Bonazzi D, Lautenschlaeger F, Piel M. Methods for two-dimensional cell confinement. Methods Cell Biol. 2014; 121:213–29. https://doi.org/10.1016/B978-0-12-800281-0.00014-2 PMID: 24560512

40. Dumont S, Mitchison TJ. Compression regulates mitotic spindle length by a mechanochemical switch at the poles. Curr Biol. 2009; 19(13):1086–95. Epub 20090618. https://doi.org/10.1016/j.cub.2009.05.056 PMID: 19540117

41. Guild J, Ginzberg MB, Hueschen CL, Mitchison TJ, Dumont S. Increased lateral microtubule contact at the cell cortex is sufficient to drive mammalian spindle elongation. Mol Biol Cell. 2017; 28(14):1975–83. Epub 20170503. https://doi.org/10.1091/mbc.E17-03-0171 PMID: 28468979

42. Neahring L, Cho NH, Dumont S. Opposing motors provide mechanical and functional robustness in the human spindle. Dev Cell. 2021; 56(21):3006–18 e5. Epub 20211005. https://doi.org/10.1016/j.devcel.2021.09.011 PMID: 34614397

43. Gaglio T, Saredi A, Bingham JB, Hasbani MJ, Gill SR, Schroer TA, et al. Opposing motor activities are required for the organization of the mammalian mitotic spindle pole. J Cell Biol. 1996; 135(2):399–414. https://doi.org/10.1083/jcb.135.2.399 PMID: 8896597

44. Merdes A, Ramyar K, Vechio JD, Cleveland DW. A complex of NuMA and cytoplasmic dynein is essential for mitotic spindle assembly. Cell. 1996; 87(3):447–58. https://doi.org/10.1016/s0092-8674(00)81365-3 PMID: 8898198

45. Hueschen CL, Kenny SJ, Xu K, Dumont S. NuMA recruits dynein activity to microtubule minus-ends at mitosis. Elife. 2017;6. Epub 20171129. https://doi.org/10.7554/eLife.29328 PMID: 29185983

46. Joukov V, De Nicolo A. Aurora-PLK1 cascades as key signaling modules in the regulation of mitosis. Sci Signal. 2018; 11(543). Epub 20180814. https://doi.org/10.1126/scisignal.aar4195 PMID: 30108183

47. Kinoshita K, Noetzel TL, Pelletier L, Mechtler K, Drechsel DN, Schwager A, et al. Aurora A phosphorylation of TACC3/maskin is required for centrosome-dependent microtubule assembly in mitosis. J Cell Biol. 2005; 170(7):1047–55. Epub 20050919. https://doi.org/10.1083/jcb.200503023 PMID: 16172205

48. Gergely F, Karlsson C, Still I, Cowell J, Kilmartin J, Raff JW. The TACC domain identifies a family of centrosomal proteins that can interact with microtubules. Proc Natl Acad Sci U S A. 2000; 97(26):14352–7. https://doi.org/10.1073/pnas.97.26.14352 PMID: 11121038

49. Ben-David U, Amon A. Context is everything: aneuploidy in cancer. Nat Rev Genet. 2020; 21(1):44–62. Epub https://doi.org/10.1038/s41576-019-0171-x PMID: 31548659.

50. Nam S, Gupta VK, Lee HP, Lee JY, Wisdom KM, Varma S, et al. Cell cycle progression in confining microenvironments is regulated by a growth-responsive TRPV4-PI3K/Akt-p27(Kip1) signaling axis. Sci Adv. 2019; 5(8):eaaw6171. Epub 20190807. https://doi.org/10.1126/sciadv.aaw6171 PMID: 31457089

51. Pernas S, Tolaney SM, Winer EP, Goel S. CDK4/6 inhibition in breast cancer: current practice and future directions. Ther Adv Med Oncol. 2018; 10:1758835918786451. Epub 20180717. https://doi.org/10.1177/1758835918786451 PMID: 30038670

52. Godinho SA, Picone R, Burute M, Dagher R, Su Y, Leung CT, et al. Oncogene-like induction of cellular invasion from centrosome amplification. Nature. 2014; 510(7503):167–71. Epub 20140413. https://doi.org/10.1038/nature13277 PMID: 24739973

53. Cosenza MR, Cazzola A, Rossberg A, Schieber NL, Konotop G, Bausch E, et al. Asymmetric Centriole Numbers at Spindle Poles Cause Chromosome Missegregation in Cancer. Cell Rep. 2017; 20(8):1906–20. https://doi.org/10.1016/j.celrep.2017.08.005 PMID: 28834753

54. Gatlin JC, Matov A, Danuser G, Mitchison TJ, Salmon ED. Directly probing the mechanical properties of the spindle and its matrix. J Cell Biol. 2010; 188(4):481–9. https://doi.org/10.1083/jcb.200907110 PMID: 20176922

55. Shimamoto Y, Maeda YT, Ishiwata S, Libchaber AJ, Kapoor TM. Insights into the micromechanical properties of the metaphase spindle. Cell. 2011; 145(7):1062–74. https://doi.org/10.1016/j.cell.2011.05.038 PMID: 21703450

56. Suresh P, Long AF, Dumont S. Microneedle manipulation of the mammalian spindle reveals specialized, short-lived reinforcement near chromosomes. Elife. 2020;9. Epub 20200319. https://doi.org/10.7554/eLife.53807 PMID: 32191206

57. Hanahan D, Weinberg RA. Hallmarks of cancer: the next generation. Cell. 2011; 144(5):646–74. https://doi.org/10.1016/j.cell.2011.02.013 PMID: 21376230

58. Schindelin J, Arganda-Carreras I, Frise E, Kaynig V, Longair M, Pietzsch T, et al. Fiji: an open-source platform for biological-image analysis. Nat Methods. 2012; 9(7):676–82. Epub 20120628. https://doi.org/10.1038/nmeth.2019 PMID: 22743772